INSTITUTE OF PHYSICS PUBLISHING JOURNAL OF PHYSICS D: APPLIED PHYSICS

J. Phys. D: Appl. Phys. **38** (2005) 1415–1420 doi:10.1088/0022-3727/38/9/014

Infrared study of laser synthesized anatase TiO_2 nanopowders

M Grujić-Brojčin[1,3], M J Šćepanović[1], Z D Dohčević-Mitrović[1], I Hinić[1], B Matović[2], G Stanišić[1] and Z V Popović[1]

[1] Center for Solid State Physics and New Materials, Institute of Physics, PO Box 68, 11080 Belgrade, Serbia and Montenegro

[2] Institute of Nuclear Sciences Vinča, Belgrade, Serbia and Montenegro

E-mail: myramyra@phy.bg.ac.yu

Received 19 November 2004, in final form 1 March 2005
Published 22 April 2005
Online at stacks.iop.org/JPhysD/38/1415

Abstract

Nanosized titanium dioxide (TiO_2) is synthesized by laser-induced pyrolysis using titanium isopropoxide as a liquid precursor. The specific surface area of as-produced nanopowders measured by the Brunauer–Emmett–Teller method (BET) varies from 84 to 110 $m^2\,g^{-1}$. X-ray diffraction (XRD) and Raman scattering showed that the TiO_2 nanocrystals had an anatase structure. The grain size of the nanoparticles was estimated from scanning electron microscopy, XRD and BET measurements. The reflection spectra of nanocrystalline TiO_2 pressed pellets has been measured in the region between 80 and 1500 cm^{-1} by Fourier transform infrared spectroscopy. To interpret the experimental results, a model based on a generalized Bruggeman effective medium approximation of a dielectric function has been proposed. It is based on the polycrystalline character of TiO_2 nanoparticles including island-structure and porosity of the nanopowders, along with the anatase single crystal dielectric functions. Thus, by comparing the results of calculated and experimental infrared (IR) spectra, the values of microscopic parameters of nanocrystalline powders can be deduced.

1. Introduction

Titanium dioxide (TiO_2) is a wide band gap semiconductor, crystallizing as rutile, anatase or brookite. Due to its physical properties (including high refractive index and dielectric constant) as well as its chemical behaviour in photosensitive reactions, TiO_2 is a highly attractive material for a wide variety of industrial applications, such as photocatalysis, catalysis, charge separating devices, chemical sensors, solar cells, microelectronics and electrochemistry [1]. The synthesis and characterization of the anatase TiO_2 nanostructures (nanoparticles, thin films, nonporous materials, pellets, etc) have attracted much interest in the last few years, and have given rise to a diversity of preparation methods [1]. Among these methods the infrared (IR) laser synthesis from gas or liquid precursors, usually known as cw CO_2 laser-induced pyrolysis, offers the advantage of a clean technology, producing a fairly uniform and controllable particle size distribution [2].

Alternatively, the analysis of nanosized materials by Fourier transform IR reflectance (FTIR) spectroscopy gives information on their bulk and surface, and provide insight into the nanostructure of the material. Despite this, only a few experimental and theoretical results related to the FTIR spectra of nanosized TiO_2 in the anatase phase, especially in the far-IR region, exist in the literature. Gonzalez [3] have presented the results of far-IR reflectivity measurements on the anatase samples: single crystals and sol–gel TiO_2 nanocrystalline particles pressed into pellets. The polarization dependent single-crystal results are analysed to yield the zone-centre transverse-optical (TO) and longitudinal-optical (LO) phonon frequencies, effective charges and polariton dispersion curves of the anatase [3, 4]. The IR spectra of TiO_2 nanopowder pressed into pellets are analysed by means of an effective medium theory that incorporates the effect of surface roughness in addition to the bulk TO and LO frequencies, which determine the dielectric functions of the anatase single crystal [3]. However, the surface roughness method, appropriate for calculation of the dielectric function

[3] Author to whom any correspondence should be addressed.

of thin films, was not fully adequate for nanopowder pressed pellets.

In this paper, a new method will be proposed to interpret the experimental results. It is based on the Bruggeman and generalized Bruggeman effective medium approximation (EMA), together with the dielectric functions for the anatase single crystal. Besides the polycrystalline character of the TiO_2 nanoparticles, this method includes the porous character of the nanopowders. The model allows us to correlate the properties of experimental IR spectra with the porosity and pore shape of nanopowder pressed pellets. The spectra calculated in this way fit the experimental data very well.

Besides the IR oscillators of bulk anatase TiO_2, two weak additional modes at about 150 and 640 cm^{-1} were observed in the IR spectra of nanopowder pressed pellets. The possible origin of these modes will be discussed and correlated to the existence of Ti^{3+} sites in the anatase structure, whose presence is very important for its photocatalytic activity.

2. Experimental details

Titanium dioxide nanopowders were synthesized by laser-induced pyrolysis, using titanium isopropoxide ($Ti(OC_3H_7)_4$) as a liquid precursor. The liquid precursor was heated at temperatures ranging between 100°C and 180°C. In this process, a cw CO_2 laser (600 W) irradiates a confined stream of titanium alkoxide vapour carried into the reaction chamber by a controlled flow of ethylene (50–1200 sccm) as a carrier gas. Controlled flow rates of oxygen have been mixed with the reactants in order to make the chemical reaction more exothermic, thus reducing the laser energy requirement for the complete reactant decomposition. The as-produced powders were calcined in air for 4 h at 500°C, in order to eliminate some carbon contamination consequent to a partial cracking of ethylene [5, 6].

The specific surface area (S_{BET}) of as-grown nanopowders was determined by the Brunauer–Emmett–Teller (BET) method using nitrogen adsorption, and depends on the preparation conditions. Measured S_{BET} values for the samples labelled TIS57, TIS24 and TIS12 were 110 $m^2\,g^{-1}$, 104 $m^2\,g^{-1}$ and 84 $m^2\,g^{-1}$, respectively.

Scanning electron microscopy (SEM) images of the nanopowders were collected using a JOEL-JSM-5300 scanning microscope at 30 kV accelerating voltage. The particle size distribution was determined from a program GSD1 developed in our laboratory.

The crystal structure of the powders was investigated by x-ray diffraction (XRD) and Raman scattering experiments. The XRD measurements were carried out with a Siemens D500/D501 diffractometer using characteristic CuK_α radiation. The Raman measurements were performed at room temperature in the backscattering geometry using the 514.5 nm line of an Ar^+ laser, Jobin-Yvon U1000 monochromator and photomultiplier as a detector.

The IR reflection spectra of TiO_2 nanopowders pressed into pellets were measured at room temperature using a BOMEM-DA8 spectrometer in the spectral range between 80 and 1500 cm^{-1}.

3. Calculation of IR spectra

The calculation of IR spectra is a powerful tool for the quantitative interpretation of the experimental spectra. The EMAs of the dielectric function are often used to model the IR reflectivity of inhomogeneous media, taking into account the macroscopic volume fractions and local microstructural geometry of the material.

The IR spectrum of anatase TiO_2 nanopowders is analysed in three steps, using (i) bulk data, (ii) the polycrystalline character of the nanopowder and (iii) the porosity of the nanopowder, together with the influence of pore shape [7]. The polycrystalline character of the nanopowder is introduced by determining the dielectric function $\varepsilon_{pc}(\omega)$ from

$$\frac{1}{3}\left(\frac{\varepsilon_{\parallel}-\varepsilon_{pc}}{\varepsilon_{\parallel}+2\varepsilon_{pc}}\right)+\frac{2}{3}\left(\frac{\varepsilon_{\perp}-\varepsilon_{pc}}{\varepsilon_{\perp}+2\varepsilon_{pc}}\right)=0, \qquad (1)$$

where $\varepsilon_{\parallel}(\omega)$ and $\varepsilon_{\perp}(\omega)$ are the dielectric functions of single crystal anatase TiO_2 in two different polarizations with respect to the c axis ($E \parallel c$ and $E \perp c$). Equation (1) is deduced from Bruggeman EMA [8]. It assumes the pellet to be a nanocomposite of two fictitious isotropic materials, having dielectric functions $\varepsilon_{\parallel}(\omega)$ and $\varepsilon_{\perp}(\omega)$, with volume fractions $\frac{1}{3}$ and $\frac{2}{3}$, respectively. Both functions are determined from the shape of the reflectivity spectra of the anatase TiO_2 single crystal using a factorized form of the dielectric function [9],

$$\varepsilon=\varepsilon_1(\omega)-i\varepsilon_2(\omega)=\varepsilon_\infty\prod_n\frac{\omega_{LOn}^2-\omega^2+i\gamma_{LOn}\omega}{\omega_{TOn}^2-\omega^2+i\gamma_{TOn}\omega}, \qquad (2)$$

with TO and LO frequencies (ω_{TO} and ω_{LO}), as well as corresponding damping factors (γ_{TO}, γ_{LO}). These parameters are listed in table 1. The high frequency dielectric constant (ε_∞) is taken from [3].

As nanophase TiO_2 is a porous material with a relatively large specific surface, the porosity of the nanopowder is included in modelling its dielectric function. The best agreement between calculated and experimental results is obtained by the generalized Bruggeman EMA [8], which introduces the effect of pore shape by using the adjustable depolarization factor L for ellipsoidal voids ($L = \frac{1}{3}$ for spherical cavities and $\frac{1}{3} < L < 1$ for prolate spheroidal cavities):

$$\left(\frac{\varepsilon_{pc}-\varepsilon_{eff}}{\varepsilon_{eff}+L(\varepsilon_{pc}-\varepsilon_{eff})}\right)f_{TiO_2}+\left(\frac{\varepsilon_{air}-\varepsilon_{eff}}{\varepsilon_{eff}+L(\varepsilon_{air}-\varepsilon_{eff})}\right)f_{air}=0. \qquad (3)$$

The porous nanopowder with the dielectric function ε_{eff} is assumed to be a nanocomposite of polycrystalline TiO_2 (with dielectric function ε_{pc} from equation (2)) and air ($\varepsilon_\infty = 1$), with volume fractions f_{TiO_2} and f_{air}, respectively. Note that $f_{air} = 1 - f_{TiO_2}$, expressed in per cent, corresponds to the macroscopic value of the nanopowder porosity.

Figure 1(a) shows the simulated reflection spectra using the generalized Bruggeman EMA for the volume fraction of the nanopowder in the range $0.55 < f_{TiO_2} < 0.80$ and for a specific depolarization factor ($L = 0.65$). In figure 1(b) the calculated spectra are presented for a specific volume fraction of the nanopowder ($f_{TiO_2} = 0.68$) varying the shape of the pores from spherical to completely elongated ($L = 0.33$–0.90). These

Table 1. The characteristic TO and LO phonon frequencies and damping factors (in cm^{-1}) of the anatase TiO_2, obtained from the fitting procedure for three samples (TIS57, TIS24 and TIS12) and the published experimental [4] and theoretical [15] results. Corresponding fitting parameters f_{TiO_2} and L are also listed for each nanopowder, as well as the TO and LO phonon frequencies for the additional weak IR modes.

	Experimental[a]						Published results			
	TIS57		TIS24		TIS12		Experimental[b]			Theory[c]
Mode	Frequency ω	Damping γ	Frequency ω	Damping γ	Frequency ω	Damping γ	Frequency ω	Damping γ	ε_∞	Frequency ω
A_{2u}										
TO	347	50	340	50	343	50	367	68	5.41	375.3
LO	755	100	340	100	720	100	755	79		743.1
$E_u(1)$										
TO	272	60	272	54	270	50	262	36	5.82	248.6
LO	365	2.8	365	2	365	2	366	4.1		340.6
$E_u(2)$										
TO	438	50	438	58	438	70	435	32		479.9
LO	850	100	850	100	850	100	876	33		892.2
Additional modes										
TO	150	100	150	120	150	90				
LO	165	105	165	165	165	98				
TO	640	230	650	180	640	200				
LO	650	250	640	220	645	230				
Fitting parameters	TIS57		TIS24		TIS12					
f_{TiO_2}	0.66		0.68		0.705					
L	0.65		0.65		0.655					

[a] This work, [b] [4], [c] [15].

results illustrate the influence of the parameters f_{TiO_2} and L on the main features of the simulated IR spectra. Generally, a decrease in TiO_2 volume fraction results in a decrease in the IR reflectivity due to greater air fraction in the powder. From figure 1(*a*) it is obvious that a decrease in f_{TiO_2} also causes a broadening of IR features. The physical reason for such behaviour lies in the fact that the smaller f_{TiO_2} is, i.e. the greater the porosity, the smaller the particle size. Namely, it is well known that spreading of spectral features is presumably due to the anharmonicity effects [10] with decreasing grain size. Increase in the factor L (figure 1(*b*)) produces similar effects on IR spectra calculated by our model, but this does not have a satisfactory physical explanation. Note that in these calculations the frequencies and damping factors correspond to IR modes of the sample TIS24 listed in table 1.

4. Results and discussion

The SEM image of the TIS57 nanopowder and the corresponding grain size distribution are presented in figures 2(*a*) and (*b*), respectively. The grain size distribution and the average grain diameter $\langle d \rangle$ are obtained from image analysis using program GSD1. As can be seen from the micrograph, most of the particles in this sample have a spherical shape, with the average grain diameter $\langle d \rangle = 39$ nm, where the grains are mostly distributed in the diameter range from 20 to 45 nm. The images of the other two samples, TIS24 and TIS12, are also analysed and their grain size distributions are shown in figures 2(*c*) and (*d*), respectively. The sample TIS24 has the greatest number of the grains of dimensions from 20 to 55 nm, grouped around the average grain diameter $\langle d \rangle = 41$ nm. The sample TIS12 with $\langle d \rangle = 44$ nm has a different size distribution in comparison with the previous two samples. This sample has almost no grains with dimensions below 30 nm, while the number of the particles decreases as the grain size increases.

XRD spectra of these nanopowders are shown in figure 3. Characteristic diffraction peaks for the anatase phase are present in all the samples. The existence of weak peaks at about $2\theta = 30^\circ$ in the XRD spectra of TIS12 and TIS24 point to the exceptionally small amount of the brookite phase, while the rutile phase was not observed in any specimen. The average grain size is roughly estimated from the major XRD peak for the anatase phase (around $2\theta = 25.3^\circ$) using the Sherrer formula: 14 nm for TIS57, 16 nm for TIS24 and 23 nm for TIS12. These values coincide with the grain sizes obtained from BET measurements performed on as-grown powders: 14 nm, 15 nm and 19 nm, respectively. The agreement between XRD and BET results suggests that the particles of as-grown powders probably consisted of single crystals [11]. The greater dimension of the grains observed recently by SEM is the consequence of the subsequent agglomeration. Also, note that a higher degree of agglomeration can be seen in the samples with smaller grain size.

Raman spectra of the samples, presented in figure 4, also confirm the anatase phase of these TiO_2 nanopowders. Namely, all observed Raman modes can be assigned to the Raman spectra of the anatase single crystal: $\sim$145 cm^{-1} (E_g), 197 cm^{-1} (E_g), 399 cm^{-1} (B_{1g}), 513 cm^{-1} (A_{1g}), 519 cm^{-1} (B_{1g}) and 639 cm^{-1} (E_g) [12]. Although the spectra were measured under the same experimental conditions, Raman modes of the sample TIS12 have the greatest intensities, while the intensities of TIS57 Raman modes are the smallest. Both phonon confinement and non-stoichiometry effects should be taken into account to explain the change in intensity and evident mode broadening [12–14].

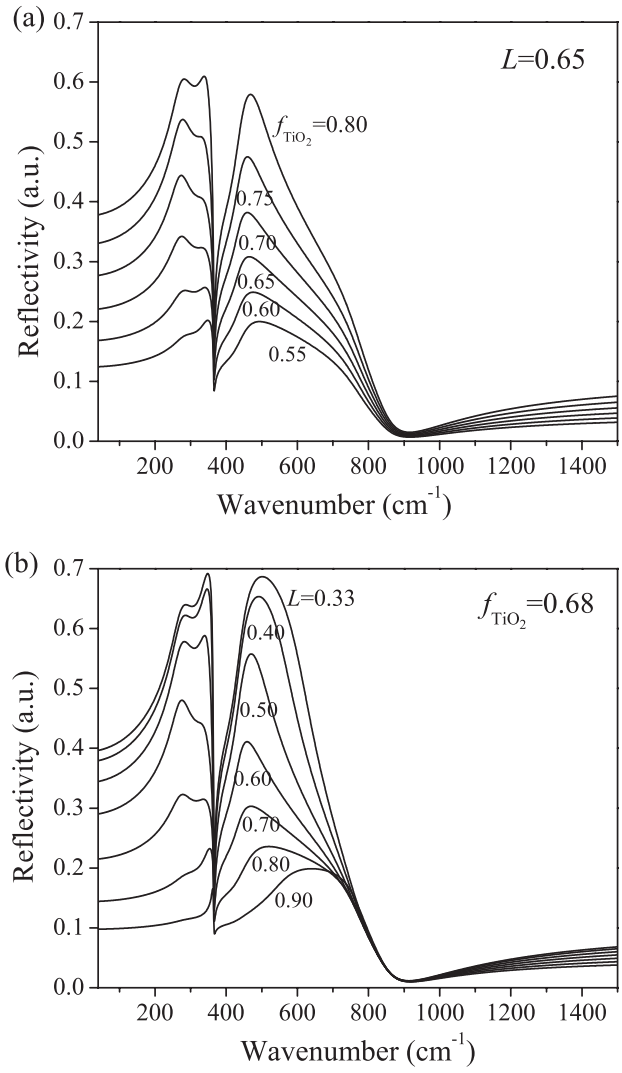

Figure 1. The simulated IR reflectivity spectra for (*a*) the volume fraction of nanopowder in the range $0.55 < f_{TiO_2} < 0.75$ and depolarization factor $L = 0.65$; (*b*) the volume fraction $f_{TiO_2} = 0.68$ and depolarization factor $L = 0.33$–0.90.

Figure 5 shows the measured IR reflection spectra (open circles) of TIS57, TIS24 and TIS12 samples together with the fitted spectra (solid line) obtained by generalized Bruggeman EMA as described in the previous paragraph. Fitting parameters for these spectra are listed in table 1. As can be seen, there is a small variation in frequencies and damping parameters for TO (LO) modes of different samples. Note, also, that the TO and LO frequencies are similar to the published experimental [4] and theoretical [15] results for the anatase single crystal, while the damping factors are greater for most of the oscillators. This could be expected because the damping factors of the oscillators in nanosized materials are usually greater than in the bulk.

On the other hand, the value of the parameter f_{TiO_2} varies from 0.66 (sample TIS57) to 0.705 (sample TIS12). This means that the porosity obtained from the fitting procedure decreases from TIS57 to TIS12. This is in agreement with the trend of specific surface area and grain size values obtained for these samples. The values of the factor L are similar for all the samples (about 0.65) indicating that the pore shape is approximately the same.

Gonzalez [3] proposed a model for analysis of the IR spectrum of sol–gel synthesized TiO_2 nanopowders pressed into pellets, where the fitted spectrum was obtained by Bruggeman EMA and the thickness of the surface roughness layer was introduced as a fitting parameter. Although the main features of experimental spectra are seen, this model does not give good quantitative agreement with experimental results for porous nanopowders. The model presented in this work, besides showing better agreement, has an important advantage: this is related to the microstructural characteristics of nanopowders, such as the porosity of the nanopowder and shape of nanoparticles and pores. Therefore, it is more suitable for the interpretation of the IR spectra of porous nanomaterial.

Besides the main features in the IR spectra, there is an appearance of two additional weak IR modes at about 150 and 640 cm^{-1} in all spectra presented in figure 5. Therefore, a good quantitative agreement between fitted and experimental results is obtained by introducing two additional oscillators in the fitting procedure. The TO (LO) frequencies of these modes are around 150 (165) and 640 (650). Note that neither the TiO_2 crystal modifications nor the other titanium oxides (such as TiO, Ti_2O_3, Ti_2O_5) and suboxides have IR active modes at these frequencies. Gonzalez *et al* [4] have registered the appearance of a weak mode, 640 cm^{-1}, in the anatase single crystal, although he claimed that the origin of this mode is still unexplained. Therefore, we tried to explain the origin of these additional modes as a consequence of lattice distortion of the anatase structure.

Anatase TiO_2 is tetragonal with the $I4_1/amd(D_{4h}^{19})$ space group [15], containing two formula units (six atoms) per primitive unit cell. From the factor group analysis, there are six Raman active modes ($A_{1g} + 2B_{1g} + 3E_g$) and three IR active modes ($A_{2u} + 2E_u$). The E_g Raman modes originate from oxygen vibrations. According to our opinion, the additional modes can be understood in terms of IR-forbidden modes [16], since the oscillator frequencies are very similar to the two strongest E_g modes in the Raman spectrum of anatase TiO_2. Actually, the existence of a small amount of Ti^{3+} substituted on Ti^{4+} sites locally may remove the neutrality of charges in the E_g vibrational modes, causing a slight lattice distortion and appearance of IR-forbidden modes. The Ti^{3+} states in the TiO_2 lattice originate from nonstoichiometry, oxygen deficiency and ion intercalation, as well as surface adsorbed species and other surface or interface states [17]. It is known that there is a tendency of anatase TiO_2 despite its high lattice energy, to release a small fraction of surface oxygen [18] followed by yellow colouring [19]. In fact, we observed that our samples became slightly yellow coloured after being pressed into pellets, indicating the presence of a small amount of Ti^{3+} sites. From the above discussion, we concluded that the existence of additional modes in the IR spectra of anatase TiO_2 nanopowders can be correlated to the presence of oxygen vacancies at the surface of crystalline nanoparticles and, consequently, to the existence of the Ti^{3+} sites in the lattice of this material. Note that Ti^{3+} surface states of TiO_2 act as a photocatalytic active site for photocatalytic reduction, and the increase in the photocatalytic activity of TiO_2 is due to the increase in Ti^{3+} concentration occurring as a result of valence change of Ti ions from Ti^{4+} to Ti^{3+} [20].

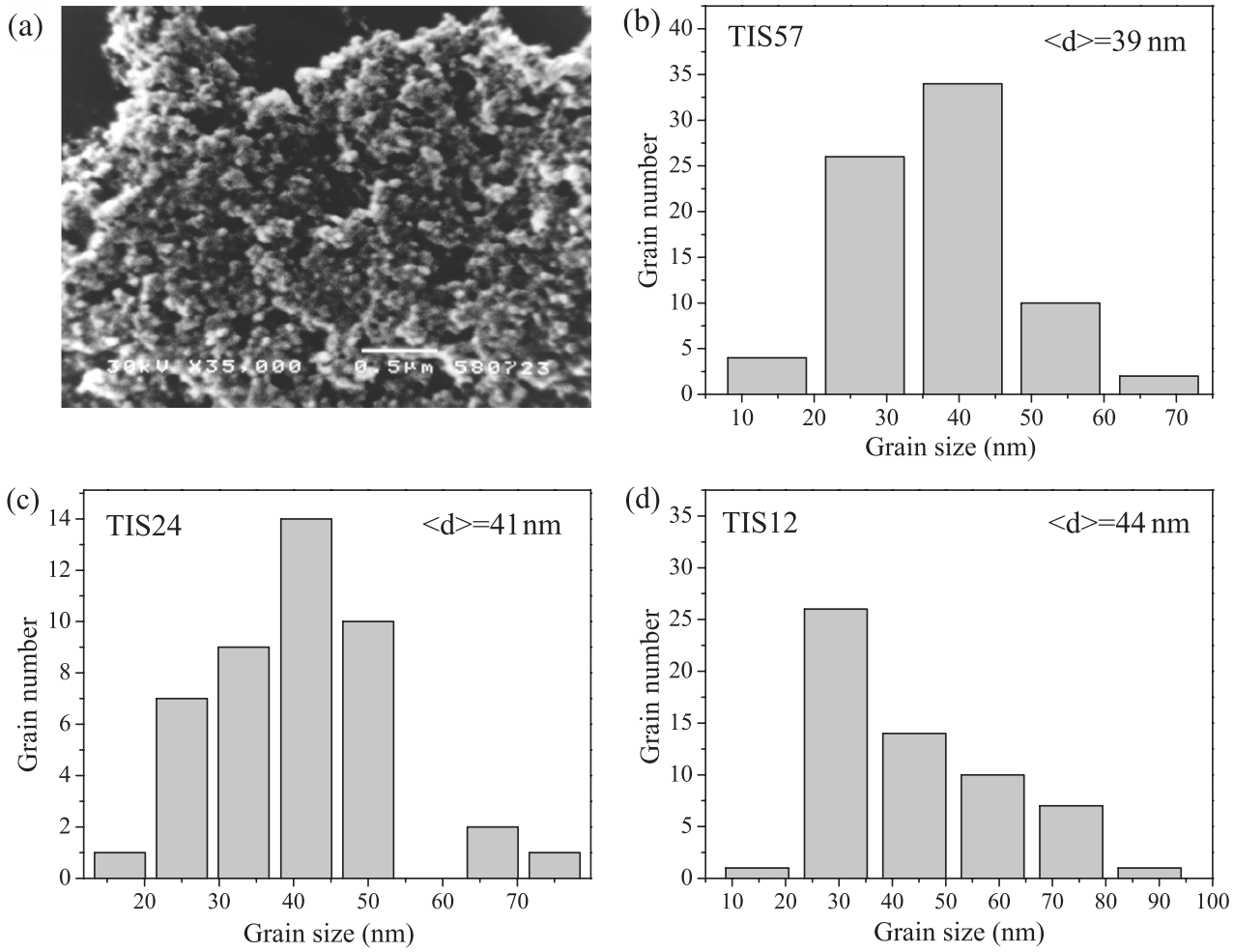

Figure 2. SEM micrographs of TiO_2 nanopowders TIS57 (*a*). The particle size distribution with the average grain diameter $\langle d \rangle$ of TIS57 (*b*), TIS24 (*c*), TIS12 (*d*).

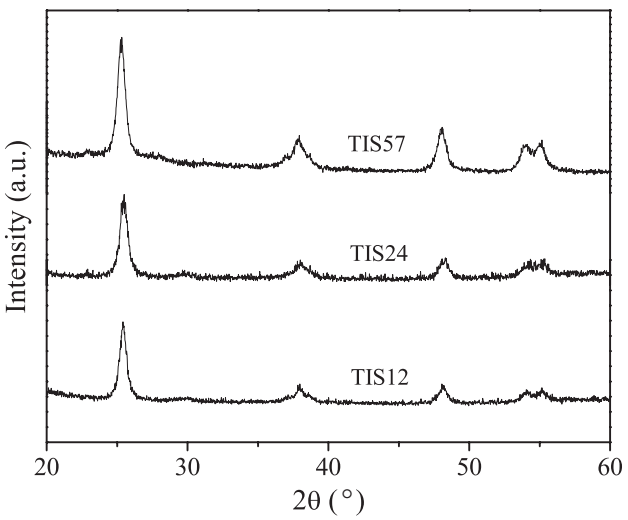

Figure 3. XRD spectra of TiO_2 nanopowder samples.

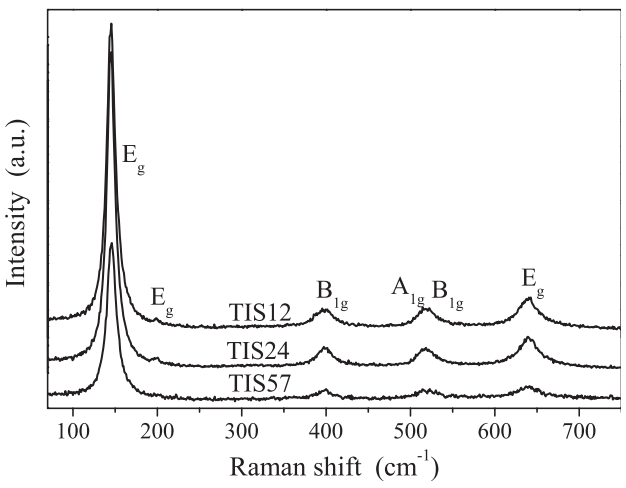

Figure 4. Raman spectra of TiO_2 nanopowder samples.

5. Conclusion

Anatase TiO_2 nanopowders, synthesized by laser-induced pyrolysis, were studied by FTIR reflection spectroscopy. The dielectric function was modelled using the Bruggeman EMA to account for the polycrystalline and porous character of the nanopowder. Comparison of reflectivity spectra calculated using this dielectric function with the experimental ones enable us to obtain the values of the main fitting

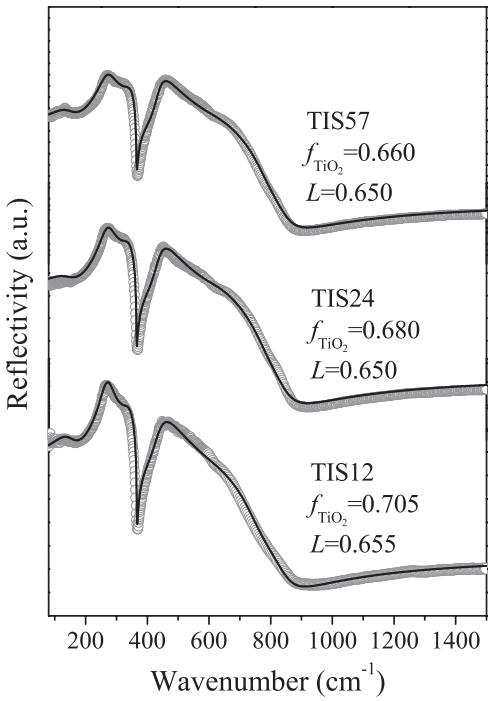

Figure 5. Experimental IR spectra (○) of the TIS12, TIS24 and TIS57 samples and fitted spectra (——) obtained by generalized Bruggeman EMA.

parameters, namely the TO and LO mode frequencies and their damping factors as well as the volume fraction of TiO_2 (air) in nanopowders. The results obtained show relatively small deviations in frequencies as well as greater damping factors relative to the corresponding oscillator parameters in bulk anatase. This is consistent with the nanocrystalline structure of TiO_2 powders. Calculated values for volume fractions of TiO_2 (air) in nanopowders are in accordance with their specific surface area and grain size values. Good qualitative and quantitative agreement between theoretical and experimental spectra and compatibility of the fitting results with the physical properties of TiO_2 nanopowders as well, confirm the validity of the proposed model.

Acknowledgment

This work is supported by the Serbian Ministry of Science and Environment Protection, under contract 1469.

References

[1] Alexandrescu R, Dumitrache F, Morjan I, Sandu I, Savoiu M, Voicu I, Fleaca C and Piticescu R 2004 *Nanotechnology* **15** 537
[2] Cannon W R, Danforth S C, Flint J H, Haggerty J S and Mara R A 1982 *J. Am. Ceram. Soc.* **65** 324
[3] Gonzalez R J 1996 Raman, infrared, x-ray, and EELS studies of nanophase titania *PhD Thesis* Virginia Polytechnic Institute
[4] Gonzalez R J, Zallen R and Berger H 1997 *Phys. Rev.* B **55** 7014
[5] Curcio F, Musci M, Notaro N and Nannetti C 1989 *Appl. Surf. Sci.* **36** 52
[6] Dohcevic-Mitrovic Z D, Šćepanović M J, Hinić I I and Stanišić G M 2004 *Mater. Sci. Forum* **453–454** 237
[7] Spanier J E and Herman I P 2000 *Phys. Rev.* B **61** 10437
[8] Bruggeman D A G 1935 *Ann. Phys.* **24** 636
[9] Gervais F 1983 *Infrared and Millimeter Waves* vol 8, ed K J Button (New York: Academic)
[10] Hayashi S and Kanamori H 1980 *J. Phys. C: Solid State Phys.* **13** 1529
[11] Nakade S, Saito Y, Kubo W, Kitamura T, Wada Y and Yanagida S 2003 *J. Phys. Chem.* B **107** 8607
[12] Zhang W F, He Y L, Zhang M S, Yin Z and Chen Q 2000 *J. Phys. D: Appl. Phys.* **33** 912
[13] Bersani D, Lottici P P and Ding X Z 1998 *Appl. Phys. Lett.* **72** 73
[14] Parker J C and Siegel R W 1990 *Appl. Phys. Lett.* **57** 27
[15] Mikami M and Nakamura S 2002 *Phys. Rev.* B **66** 155213-1
[16] Gervais F and Piriou B 1974 *Phys. Rev.* B **10** 1642
[17] Eppler A M, Ballard I M and Nelson J 2002 *Physica* E **14** 197
[18] Weidmann J, Dittrich Th, Konstantinova E, Lauermann I, Uhlendorf I and Koch F 1999 *Sol. Energy Mater. Sol. Cells* **56** 153
[19] Zhu X and Meng Z 1994 *J. Appl. Phys.* **75** 3756
[20] Yu J, Zhao X and Zhao Q 2001 *Mater. Chem. Phys.* **69** 25